J Appl Physiol 96: 1832–1842, 2004.
First published January 16, 2004; 10.1152/japplphysiol.01157.2003.

Characterizing airway and alveolar nitric oxide exchange during tidal breathing using a three-compartment model

Peter Condorelli,[1,2] Hye-Won Shin,[1] and Steven C. George[1,2]
Departments of [1]Biomedical Engineering and [2]Chemical Engineering and Materials Science, University of California, Irvine, California 92697-2575

Submitted 28 October 2003; accepted in final form 29 December 2003

Condorelli, Peter, Hye-Won Shin, and Steven C. George. Characterizing airway and alveolar nitric oxide exchange during tidal breathing using a three-compartment model. *J Appl Physiol* 96: 1832–1842, 2004. First published January 16, 2004; 10.1152/japplphysiol.01157.2003.—Exhaled nitric oxide (NO) may be a useful marker of lung inflammation, but the concentration is highly dependent on exhalation flow rate due to a significant airway source. Current methods for partitioning pulmonary NO gas exchange into airway and alveolar regions utilize multiple exhalation flow rates or a single-breath maneuver with a preexpiratory breath hold, which is cumbersome for children and individuals with compromised lung function. Analysis of tidal breathing data has the potential to overcome these limitations, while still identifying region-specific parameters. In six healthy adults, we utilized a three-compartment model (two airway compartments and one alveolar compartment) to identify two potential flow-independent parameters that represent the average volumetric airway flux (pl/s) and the time-averaged alveolar concentration (parts/billion). Significant background noise and distortion of the signal from the sampling system were compensated for by using a Gaussian wavelet filter and a series of convolution integrals. Mean values for average volumetric airway flux and time-averaged alveolar concentration were 2,500 ± 2,700 pl/s and 3.2 ± 3.4 parts/billion, respectively, and were strongly correlated with analogous parameters determined from vital capacity breathing maneuvers. Analysis of multiple tidal breaths significantly reduced the standard error of the parameter estimates relative to the single-breath technique. Our initial assessment demonstrates the potential of utilizing tidal breathing for noninvasive characterization of pulmonary NO exchange dynamics.

gas exchange; pulmonary; mathematical model

MEASUREMENT OF EXHALED, ENDOGENOUS nitric oxide (NO) has been proposed as a noninvasive technique for assessment of pulmonary inflammation (4). Exhaled NO concentration is highly dependent on flow rate due to a significant airway source (11, 22, 28). This finding has led to the development of a two-compartment model of the lungs that partitions exhaled NO into airway and alveolar contributions by using a series of flow-independent NO exchange parameters: airway diffusing capacity (Daw_{NO}), maximum airway flux ($J'_{aw\ NO}$), and steady-state alveolar concentration (C_{ANO}) (10, 17, 23, 26, 27). Several groups have utilized single-breath (i.e., vital capacity) maneuvers to estimate the flow-independent NO parameters in health and disease and have reported altered NO exchange dynamics in several inflammatory lung diseases (e.g., asthma, cystic fibrosis, allergic alveolitis, scleroderma, and chronic obstructive pulmonary disease) (7, 10, 15, 19, 20, 23). Application of the two-compartment model during tidal breathing has not been explored but may be applicable for young children, intubated subjects, and subjects with compromised lung function who are unable to perform the single-breath maneuvers (6, 24).

Analysis of tidal breathing data presents new challenges relative to single-breath maneuvers. Smaller changes in lung volume are often inadequate to overcome sampling system limitations, such as dead space in sampling system plumbing. Each breath occurs over shorter time intervals, which allows less time for NO to accumulate in the airways, compared with single-breath maneuvers. This leads to expired NO levels, which are significantly less than those observed for single-breath maneuvers (1, 8). Analysis of multiple consecutive tidal breaths may partially offset these limitations.

Herein, we characterize NO gas exchange during tidal breathing in terms of two flow-independent parameters: the average volumetric conductive airway flux ($\bar{J}_{aw\ NO}$) and the time-averaged alveolar concentration ($\bar{C}_A$). We hypothesize that $\bar{J}_{aw\ NO}$ and $\bar{C}_A$ serve as indexes for NO exchange dynamics in the airway and alveolar regions, respectively. As a first step, these parameters are estimated by comparison of experimental tidal breathing exhalation profiles in healthy adults with the use of a new three-compartment model, which includes two airway sections and one alveolar compartment. Estimates of $\bar{J}_{aw\ NO}$ and $\bar{C}_A$ are compared with analogous parameters determined by using a previously described single-breath technique and the two-compartment model (26, 27): $J'_{aw\ NO}$ and C_{ANO}. Our analysis includes correction of the experimental data for time lags and distortion introduced by the analytic monitoring system. These effects are insignificant for single-breath maneuvers, but profoundly impact low-level tidal breathing data.

Glossary

B = Correction for baseline drift, fitted to $\bar{C}_{I,out}(t)$ [parts/billion (ppb)]
C = Gas-phase NO concentration (ppb)
$\bar{C}$ = Time-weighted average gas-phase NO concentration (ppb)
Daw_{NO} = Airway diffusing capacity ($ml \cdot s^{-1} \cdot ppb^{-1}$, $pl \cdot s^{-1} \cdot ppb^{-1}$)
$E_s(t)$ = $\int_0^{t_{E_m}+t_{I_{m+1}}} \psi_s(t,u)du$, where du is a differential increment in the dummy variable u.
f_B = $1/(t_I + t_E)$ = breathing frequency (breaths/min, s^{-1}, min^{-1})
$G_j(t)$ = Functions (j = 1, 2, 3): $C_{I,out}(t) = J_{aw\ NO,U}\ G_1(t) + J_{aw\ NO,L}\ G_2(t) + \bar{C}_A\ G_3(t)$

Address for reprint requests and other correspondence: S. C. George, Dept. of Chemical Engineering and Materials Science, 916 Engineering Tower, Univ. of California, Irvine, Irvine, CA 92697-2575 (E-mail: scgeorge@uci.edu).

The costs of publication of this article were defrayed in part by the payment of page charges. The article must therefore be hereby marked "*advertisement*" in accordance with 18 U.S.C. Section 1734 solely to indicate this fact.

$\bar{G}_j(t)$ = Functions (j = 1, 2, 3): $\bar{C}_{I,out}(t) = J_{aw\,NO,U}\,\bar{G}_1(t) + J_{aw\,NO,L}\,\bar{G}_2(t) + \bar{C}_A\,G_3(t) + B$
$J_{aw\,NO}$ = $J'_{aw\,NO} - Daw_{NO}\,C_{air}$ = net NO flux into airway compartment air space (pl/s, ml/s)
$J'_{aw\,NO}$ = Maximum volumetric airway flux (pl/s, ml/s)
$\bar{J}_{aw\,NO}$ = $(Vaw_U\,J_{aw\,NO,U} + Vaw_L\,J_{aw\,NO,L})/Vaw$ = time and volume-weighted average of $J_{aw\,NO}$ over entire airway compartment, where $J_{aw\,NO,U}$ and $J_{aw\,NO,L}$ are the averages of $J_{aw\,NO}$ over the upper 10% and lower 90% of the airway compartment volumes, Vaw_U and Vaw_L, respectively, for a single exhalation (pl/s, ml/s)
M = Total number of tidal breaths observed in an exhalation profile sequence
N_m = Number of sampled concentrations in tidal breath m
q = Q_I/Q_E = inhalation-to-exhalation flow rate ratio
Q = Volumetric, air, flow rate = $-Q_I$ (inhalation), Q_E (exhalation) (ml/s)
s_{xj}, s_{yj} = Standard deviation of input, x_j, or output, y_j, respectively
t = Time or time interval (s)
V = Volume or axial position in units of cumulative volume (ml)
$\dot{V}_A$ = $(Q_E\,t_E - Vaw)\,f_B$ = alveolar ventilation rate, mean for M breaths (ml/s or l/min)
$\psi_s(t,u)$ = $e^{-0.5[(u\,-\,t)/s]^2}/(s\sqrt{2\pi})$, where s is scaling factor for wavelet transform (s)
σ_j = Uncertainty of parameter estimate ($j = \bar{J}_{aw\,NO}$, $\bar{C}_A$)
τ = Residence time, space time, or time constant (s)

Modifiers

a, air,
or aw = Airway compartment or airway gas space
A = Analyzer [time constant for NO analyzer's response (first-order system)]
A = Alveolar compartment
ds = Dead space
E = Exhalation
I = Inhalation or instrument
I,in = Input to NO analyzer (instrument)
I,out = NO analyzer response (output)
j = Index for parameters; $\bar{J}_{aw\,NO}$ (j = 1) and $\bar{C}_A$ (j = 2) or general integer
L = Lower 90% of airway compartment volume
m = Index for tidal breaths, m = 1, 2, . . . M (M = total tidal breaths)
M = NO profile at the mouth
n = Index for data samples (n = 0, 1, 2, . . . N_m; in tidal breath m)
obs = Observed (experimental) profile (signal)
s = Sample line or sample point
U = Upper 10% of airway compartment volume

METHODS

Experimental protocol. Six healthy, nonsmoking adults with no prior history of lung disease participated in the study. The Institutional Review Board at the University of California, Irvine approved the protocol, and written informed consent was obtained from all subjects. Each subject performed two different breathing maneuvers. First, each subject completed a single exhalation with a 20-s preexpiratory breath hold, followed by a decreasing exhalation flow rate (Q_E) (from ~6 to ~1% of vital capacity per second) in triplicate, as previously described (27). From these data, we determined the corresponding values of $J'_{aw\,NO}$, C_{ANO}, and Daw_{NO} using nonlinear regression (27). For preexpiratory breath-hold maneuvers, a positive pressure of >5 cmH_2O was maintained to prevent nasal contamination, and a Starling resistor (Hans Rudolph, Kansas City, MO) was used to progressively decrease the flow rate during exhalation.

Second, after allowing 1 min of comfortable tidal breathing before collection of data, each subject breathed comfortably in a tidal fashion for a minimum of 3 min (maximum of 5 min). NO was scrubbed from ambient air by using a filter (Ionics, Boulder, CO) to produce "NO-free air," which was used as the inhaled gas. Exhaled NO concentration and flow rate were measured at breathing frequencies of 7–15 breaths/min and alveolar ventilation ($\dot{V}_A$) rates of 6–13 l/min (see Table 2). Subsequently, $\bar{J}_{aw\,NO}$ and $\bar{C}_A$ were determined from the tidal breathing data (see below for details).

After NO collection, standard spirometric indexes were measured (Vmax229; Sensormedics, Yorba Linda, CA), which included forced vital capacity and forced expiratory volume in 1 s, based on the best performance from three consecutive measurements. All data were obtained with the subjects in the upright position. Table 1 summarizes each subject's physical characteristics, standard spirometry measurements, and conducting airway volumes (Vaw), estimated based on age and ideal body weight (20).

The experimental monitoring system is shown in Fig. 1*A*, which measures NO concentration in real-time using a chemiluminesent NO analyzer (NOA280, Ionics), and measures volumetric flow rate and pressure with a pneumotachometer (model RSS100, Hans Rudolph). A digital computer collects data for all three signals at 50 Hz (sampling time = 0.02 s).

Sampling system model. During exhalation (flow rate, $Q_{E\,m}$, and time interval, $0 < t < t_{E\,m}$, for breath m), air from the mouth [NO concentration, $C_M(t)$] traverses the mouthpiece assembly entrance dead space (volume, $V_{ds\,1}$ = 135 ml, see Fig. 1), on its way to the sampling point [NO concentration, $C_s(t)$]. At the sampling point, a small flow of air (Q_s = 4.2 ml/s) is collected by the chemiluminescent NO analyzer continuously through a 1.8-mm-diameter sample line (total volume, V_s = 5.5 ml, and space time, $\tau_s = V_s/Q_s \approx 1.3$ s). Although NO is sampled upstream of the pneumotachometer, Q_s is small (<5%), relative to $Q_{E\,m}$, and the impact of this flow rate on parameter estimates is insignificant. On subsequent inhalation (flow, $Q_{I\,m+1}$, and $t_{E\,m} < t$, for breath m + 1), NO-free air is not present at the sampling point until inspired air traverses the mouthpiece assembly exit dead space (volume, $V_{ds\,2}$ = 135 ml). Lag times in both dead space regions are approximated by their respective space times: $\tau_{ds\,1m} = V_{ds\,1}/Q_{E\,m}$ and $\tau_{ds\,2,m+1} = V_{ds\,2}/Q_{I\,m+1}$. Thus, during exhalation, the $C_s(t)$ lags the mouth in accordance with the relationship, $C_s(t) = C_M(t - \tau_{ds\,1m})$, and on subsequent inhalation, residual

Table 1. *Physical characteristics of subjects*

Subject No.	Gender	Age, yr	Height, in.	Weight, lb.	Vaw, ml	FVC liter	FVC %	FEV_1/FVC, %
1	M	37	69	145	191	4.65	95	80
2	F	27	64	119	155	3.55	99	89
3	M	22	73	171	193	5.09	89	83
4	M	37	70	165	197	4.39	85	79
5	M	30	67	163	178	4.94	106	87
6	M	21	70	201	179	4.79	94	83
Mean		29	69	161	153	4.57	95	84
SD		7	3	27	15	0.55	7	4

M, male; F, female; Vaw, airway compartment volume; FVC, forced vital capacity, expressed in liters or %predicted; FEV_1, forced expiratory volume in 1 s (% of FVC). Vaw = (ideal body weight, lb.) + (age, yr) (20).

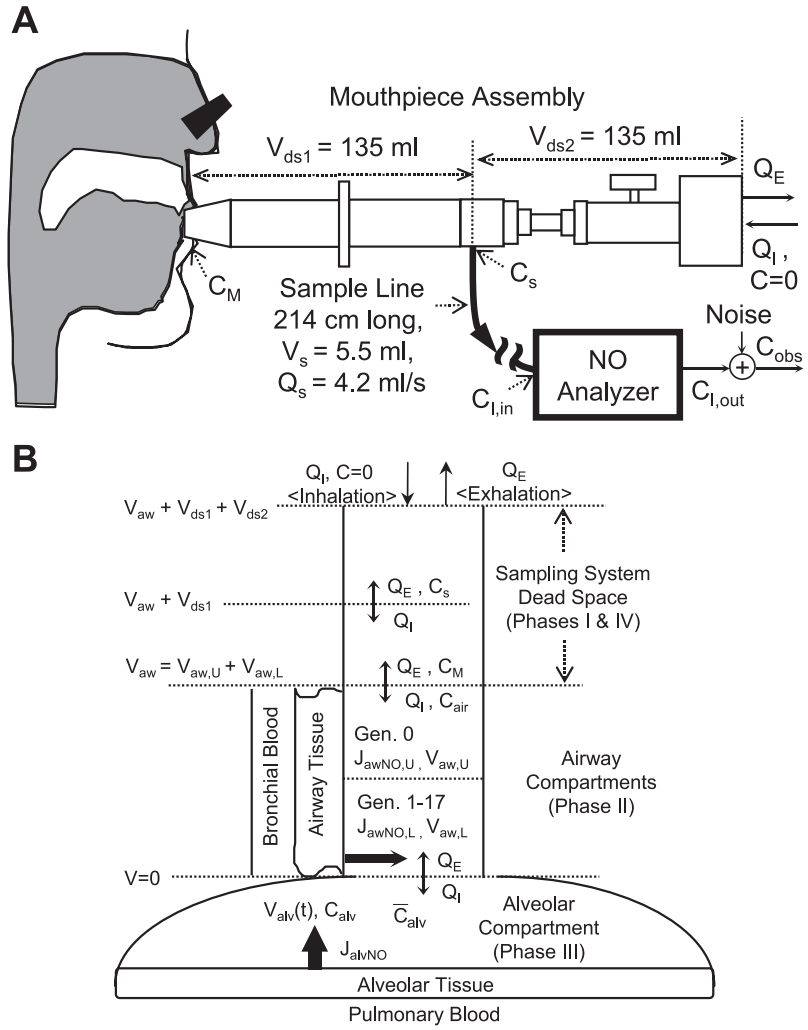

Fig. 1. Schematic representation of sampling system, showing dead space volumes, sample line, and nitric oxide (NO) analyzer (*A*), and lung model, showing airway, alveolar, and sampling system compartments (*B*). Exhaled NO has sources in both the alveolar (J_{ANO}) and the airway (J_{awNO}) regions of the lungs. The airway compartment has been divided into an upper airway (subscript U) and a lower airway (subscript L) compartment; thus the lung model used to analyze a tidal breath has 3 compartments (two airway compartments and one alveolar compartment). See *Glossary* for definition of terms. alv, Alveolar (A).

NO is sampled [i.e., baseline, $C_s(t) = 0$, is not established] until time $t = t_{E\,m} + \tau_{ds\,2,m+1}$.

Because the sample line is maintained at laminar flow (Reynolds number is ~180 and laminar flow occurs for Reynolds numbers <2,100 in cylinders), air at the tube centerline moves approximately twice as fast as the average bulk flow. This effect significantly delays and distorts the concentration profile input to the NO analyzer (instrument), $C_{I,in}(t)$, which is approximated as a convolution integral of $C_s(t)$, defined by *Eqs. A5* and *A6* in APPENDIX A (3). At the analyzer, the instrument's response, $C_{I,out}(t)$, is approximated as a first-order system with time constant $\tau_A = 90$ ms (see *Eq. A7* in APPENDIX A), as reported by the manufacturer (Ionics). $C_{I,out}(t)$ then corresponds to a theoretically predicted tidal breathing profile, based on the lung models, as discussed below.

Two-compartment lung model. The two-compartment model has been described previously in detail by several research groups, including ours (10, 17, 23, 26), and is currently the accepted model of NO gas exchange. Thus it is the starting point for our analysis of tidal breathing. Briefly, the model approximates the conducting airways (i.e., the trachea and the first 17 airway generations) as a rigid, cylindrical compartment of volume, Vaw, and axial diffusion is neglected. The respiratory bronchioles and alveolar region (*generations 18* and beyond) expand and contract to accommodate inspired and expired air. Endogenously produced NO diffuses into the airway compartment at net flux ($J_{aw\,NO}$). These assumptions lead to a differential mass balance for the airway gas-phase concentration of NO, $C_{air}(t,V)$ (26)

$$\frac{\partial C_{air}}{\partial t} + Q\frac{\partial C_{air}}{\partial V} = J_{aw\,NO}(C_{air}, V)/Vaw \qquad (1)$$

where t is time, V is cumulative volume, $J_{aw\,NO}$ (C_{air}, V) is the net flux of NO into the airway (a function of C_{air} and V), and Q is the volumetric flow rate of air [$Q = -Q_I(t)$ for inhalation and $Q = Q_E(t)$ for exhalation, see Fig. 1*B*].

Previous work for single-breath maneuvers (26) approximates $J_{aw\,NO}$ as a linear function of C_{air}, $J_{aw\,NO} = J'_{aw\,NO} - Daw_{NO}\,C_{air}$. If exhalation proceeds for >10 s, the alveolar concentration is assumed to reach a steady-state value (C_{ANO}) (12, 26, 27). Thus NO exchange is characterized by three flow-independent parameters: $J'_{aw\,NO}$, Daw_{NO}, and C_{ANO}. $J'_{aw\,NO}$, Daw_{NO}, and C_{ANO} were determined by using the two-compartment model and the 20-s preexpiratory breath hold and decreasing Q_E maneuver (27) for all six subjects as a basis for comparison to our characterization of NO exchange dynamics during tidal breathing.

Three-compartment lung model. In our initial analysis, the tidal breathing exhalation profile was often difficult to simulate due to a rapid increase in NO concentration early in exhalation (Phases I and II in Figs. 2–4). Thus the two-compartment model (26) was expanded for tidal breathing to include two airway sections (i.e., a three-compartment model, as shown in Fig. 1*B*). This advancement is based

on data from Tornberg et al. (24, 25), who demonstrated that the mouth and trachea contribute more exhaled NO than the lower airways by analyzing expired air from both tracheotomized and intubated, mechanically ventilated patients. Earlier studies provide further evidence for this representation. Silkoff et al. (21) demonstrated that the trachea and main bronchi contribute up to 50% of the NO appearing in the exhaled breath. In addition, Dubois et al. (5) collected and analyzed volumes of expired air from different regions of the respiratory tract to obtain data consistent with this hypothesis. Thus the local flux per unit volume is expected to be higher in the mouth and trachea than in the lower portion of the airway compartment. Time and volume-weighted averages of $J_{aw\,NO}$ are thus defined over the entire airway compartment (volume, Vaw), the upper 10% (volume, Vaw_U, represents the oropharynx and trachea), and lower 90% of the airway compartment (volume, Vaw_L) as $\bar{J}_{aw\,NO}$, $J_{aw\,NO,U}$, and $J_{aw\,NO,L}$, respectively. Hence, $\bar{J}_{aw\,NO}$ is analogous to the breath-hold parameter, $J'_{aw\,NO}$, and determined from the relationship, $\bar{J}_{aw\,NO} = (Vaw_U\,J_{aw\,NO,U} + Vaw_L\,J_{aw\,NO,L})/Vaw$, where $Vaw = Vaw_U + Vaw_L$ with the constraints, $J_{aw\,NO,U} \geq J_{aw\,NO,L} \geq 0$. As $\bar{J}_{aw\,NO} \rightarrow J_{aw\,NO,U} \rightarrow J_{aw\,NO,L}$, the three-compartment model reduces to the two-compartment model.

For healthy adult subjects, $Daw_{NO} \approx$ 1–10 pl·s^{-1}·ppb^{-1}, and $J'_{aw\,NO} \approx$ 300–2,000 pl/s (9, 17, 20, 23). These estimates for Daw_{NO} are made either following a 20-s breath hold or during Q_E <30 ml/s, in which peak NO values exceed ~70 ppb (9, 17, 22, 28). For tidal breathing, typical peak values of C_{air} range from 2 to 20 ppb; hence, in most cases, $J'_{aw\,NO}/Daw_{NO} \gg C_{air}$, and $J_{aw\,NO} \approx J'_{aw\,NO}$. Thus expired NO profiles during tidal breathing are insensitive to Daw_{NO}, making Daw_{NO} very difficult to determine for tidal breathing. Consequently, for this study, $J_{aw\,NO}$ is assumed constant with respect to time and independent of C_{air} during tidal breathing.

For single-breath maneuvers, the alveolar region is approximated as a well-mixed compartment (9, 17, 23, 26). This assumption predicts that the alveolar gas concentration, $C_A(t)$, approaches its steady-state value, $C_{A_{NO}}$, for breath-hold times exceeding 10 s. However, for tidal breathing, alveolar gas exchange is characterized by much shorter contact times, and trends in the alveolar plateau are difficult to discern, due to concentration fluctuations. Thus, for tidal breathing, $\bar{C}_A$ is defined as the time-weighted average of $C_A(t)$, over the interval, $0 < t < t_{E\,m}$ (similar to the breath-hold parameter, $C_{A_{NO}}$, but not necessarily reflecting the steady-state concentration), and $\bar{C}_{air}(t, V = 0) = \bar{C}_A$ for exhalation. In general, estimates of $\bar{J}_{aw\,NO}$ and $\bar{C}_A$ will vary with each tidal breath; however, averaging these estimates over a sequence of tidal breaths will decrease the uncertainty in the parameter estimate (e.g., smaller standard error of the estimate).

Each tidal breath is analyzed independently, and time is reset to zero at the beginning of each exhalation in a sequence of breaths, designating each breath (inhalation followed by exhalation) by the index m ($m + 1$ corresponds to subsequent inhalation). Q_I and Q_E rate profiles are approximated by their time-weighted averages, $Q_{I\,m}$ and $Q_{E\,m}$, over their respective time intervals, $t_{I\,m}$ and $t_{E\,m}$. With these assumptions, integration of *Eq. 1* leads to algebraic expressions for the exhalation profile at the mouth, $C_M(t) = C_{air}(t, V = Vaw)$, on the interval, $0 \leq t < t_{E\,m}$, expressed in terms of $Q_{I\,m}$, $Q_{E\,m}$, $t_{I\,m}$, $t_{E\,m}$, and the empirical parameters $J_{aw\,NO,U}$, $J_{aw\,NO,L}$, and C_A (see *Eqs. A1–A4* in APPENDIX A). During exhalation, $C_s(t) = C_M(t - \tau_{ds\,1m})$. At the onset of subsequent inhalation ($t_{E\,m} < t = t_{E\,m} + \tau_{ds\,2,m+1}$), $C_s(t)$ can be expressed in terms of C_M by a similar relationship (see APPENDIX A), and the baseline is assumed to be established at the sampling point [$C_s(t) = 0$] at time $t = t_{E\,m} + \tau_{ds\,2,m+1}$. Thus numerical integration of *Eqs. A5*, *A6*, and *A7* [convolution of $C_s(t)$] yields $C_{I,out}(t)$ as a linear function of $J_{aw\,NO,U}$, $J_{aw\,NO,L}$, and $\bar{C}_A$, in terms of known functions of time and breathing pattern, which are determined numerically, based on the three-compartment lung model.

Alternatively, if $C_{I,out}(t)$ is specified [e.g., the actual observed experimental data, denoted $C_{obs}(t)$], then $C_s(t)$ [and ultimately $C_M(t)$] may be determined numerically, independent of the lung model [i.e., deconvolution of $C_{obs}(t)$]. Data filtering facilitates both convolution of $C_s(t)$ (to determine $J_{aw\,NO,U}$, $J_{aw\,NO,L}$, and $\bar{C}_A$) and deconvolution of $C_{obs}(t)$ [to determine $C_s(t)$ and $C_M(t)$ directly from the experimental data], as discussed below.

Data filtering. Exhaled NO concentrations are close to the lower detection limit of the chemiluminescent analyzer, and noise introduced during the monitoring process gives rise to signal fluctuations. Criteria for removal of high-frequency noise (low-pass filtering) is based on comparison of tidal breathing signals with the corresponding baseline reading of the instrument (see APPENDIX B). Low-pass filtering involves Gaussian averaging of adjacent concentration "samples" by using the Gabor transform (13), which are applied to both $C_{obs}(t)$ and the predicted model result at the instrument, $C_{I,out}(t)$, to obtain two transformed signals, $\bar{C}_{obs}(t)$ and $\bar{C}_{I,out}(t)$, respectively (see APPENDIX B). Transformation of both signals ensures a consistent basis for parameter estimation. In addition to parameter estimates, a correction for baseline drift is applied in the fit $\bar{C}_{I,out}(t)$ to $\bar{C}_{obs}(t)$ (the constant *B*, defined in *Eq. B2*, equivalent to a high-pass filter correction).

Parameter estimation and statistical analysis. $J_{aw\,NO,U}$, $J_{aw\,NO,L}$, and $\bar{C}_A$ are determined by a least squares fit of $\bar{C}_{I,out}(t)$ to $\bar{C}_{obs}(t)$. Time windows of comparison are translated to align $\bar{C}_{obs}(t)$ and $\bar{C}_{I,out}(t)$ with each other, based on the minimum least squared error criterion, and constraints are imposed on all three parameters: $J_{aw\,NO,U} \geq J_{aw\,NO,L} \geq 0$, and $\bar{C}_A \geq 0$. Finally, the average airway flux is computed as $J_{aw\,NO} = (Vaw_U\,J_{aw\,NO,U} + Vaw_L\,J_{aw\,NO,L})/Vaw$, and for each subject, the composite average estimates of $\bar{J}_{aw\,NO}$ and $\bar{C}_A$ are reported for a sequence of *M* tidal breaths with each breath weighted equally (see APPENDIX B). The reported composite uncertainties for $\bar{J}_{aw\,NO}$ and $\bar{C}_A$ are analogous to the standard deviation (i.e., computed at 68.3% confidence intervals, as discussed in APPENDIX B). Finally, to assess the significance of the relationships between parameters characterizing preexpiratory breath hold and tidal breathing, $J'_{aw\,NO}$ and $C_{A_{NO}}$ were correlated as linear functions of the estimates for $\bar{J}_{aw\,NO}$ and $\bar{C}_A$.

There were three inclusion criteria for a tidal breath to be included in the parameter estimation algorithm. First, any tidal breath exhibiting a peak NO value early in exhalation exceeding 50 ppb was assumed to have overt nasal contamination and was removed from the analysis (denoted as "Nasal" in Table 2) (24, 25). Second, the breathing pattern is characterized by the flow rate ratio, $q_m = Q_{I\,m}/Q_{E\,m}$, breathing frequency, $f_{B\,m} = 1/(t_{I\,m} + t_{E\,m})$, and $\dot{V}_A$ rate, $\dot{V}A_m = [Q_{E\,m}\,t_{E\,m} - Vaw]f_B$. Only those breaths for which $\dot{V}A_m > [V_{ds\,1} + V_{ds\,2}]f_B$ were analyzed, which requires tidal volume changes to exceed $Vaw + V_{ds\,1} + V_{ds\,2}$, or $t_{E\,m} > \tau_{Ea\,m} + \tau_{E\,ds\,1m} + \tau_{E\,ds\,2m}$ in terms of the airway residence times for exhalation, $\tau_{Ea\,m} = Vaw/Q_{E\,m}$. This screening criterion ensures that sufficient air from the alveolar region is observed at the instrument to obtain meaningful $\bar{C}_A$

Table 2. *Characteristics of tidal breathing analysis*

Subject No.	*M*	Leak	Exh. Vol.	Nasal	Total	f_B, beats/min	$\dot{V}_A$, l/min	q
1	52	0	4	0	56	11.1	7.1	1.6
2	40	1	3	0	44	9.5	7.4	1.4
3	19	0	1	0	20	6.5	7.0	1.9
4	18	50	9	0	77	14.6	6.6	1.8
5	14	17	3	3	37	10.6	6.4	1.5
6	43	0	4	1	48	9.3	7.0	2.3
Total	186	68	24	4	282			
Mean	31				47	10.3	6.9	1.8
SD						2.7	0.4	0.3

M, no. of analyzed tidal breaths for each subject; leak, exh. vol., and nasal: no. of tidal breaths removed from analysis due to leakage of gas flow from mouthpiece, inadequate exhaled volume, and nasal contamination, respectively; f_B, mean breathing frequency (in breaths/minute); $\dot{V}_A$, mean alveolar ventilation rate (in l/min); q, ratio of inhaled to exhaled air flow = mean flow rate ratio.

estimates (denoted as "Exh. Vol." in Table 2). Third, to ensure no leakage of air from the mouthpiece (or system plumbing), tidal breaths were removed from analysis, if the calculated lung volume at end inspiration or end expiration varied by >20% (denoted as "Leak" in Table 2).

RESULTS

Theoretical tidal breathing profiles. Figure 2 depicts theoretical concentration profiles for a single tidal breath (see Fig. 2, *B–D*), at fixed $\dot{V}_{aw\,NO}$ = 2,500 pl/s (mean value from healthy adult subjects, see below) and Vaw = 200 ml, with flow rates approximated as time-weighted averages (see Fig. 2*A*), for a typical breathing pattern, corresponding to $q_m = \dot{V}_{I\,m}/\dot{V}_{E\,m}$ = 1.6, $f_{B\,m}$ = 12.8 breaths/min, and $\dot{V}_{A_m}$ = 6.7 l/min. $\dot{V}_{aw\,NO,L}$ and $\bar{C}_A$ are varied at representative values, with $\dot{V}_{aw\,NO,U}$ = (Vaw $\dot{V}_{aw\,NO}$ − Vaw_L $\dot{V}_{aw\,NO,L}$)/Vaw_U. When $\dot{V}_{aw\,NO}$ = $\dot{V}_{aw\,NO,U}$ = $\dot{V}_{aw\,NO,L}$ = 2,500 pl/s and C_A = 3.2 ppb, theoretical NO concentration profiles for the two-compartment model are obtained at the mouth, $C_M(t)$, the sampling point, $C_s(t)$, the analyzer input, $C_{I,in}(t)$, and analyzer output, $C_{I,out}(t)$ (see Fig. 2*B*). As a result of sampling system dead space, both $C_{I,in}(t)$ and $C_{I,out}(t)$ are delayed, relative to $C_M(t)$ and $C_s(t)$.

Four phases, corresponding to the observed NO exhalation profiles, $C_{I,out}(t)$, are designated by roman numerals in Fig. 2, *B* and *C*. At the beginning of exhalation, NO-free air is present at the NO analyzer, and a baseline response, denoted as phase I, is observed. The time intervals when expired air, originating from the airway and alveolar compartments, is observed are designated as phase II (*Eqs. A1* and *A2*) and phase III (*Eq. A3*), respectively. At the beginning of subsequent inhalation, residual NO is observed at the sampling point (designated as phase IV) and represents an artifact of the sampling; hence, phase IV is removed before fitting the model [$C_{I,out}(t)$] to the experimental data [$C_{obs}(t)$].

Figure 2*C* shows $C_M(t)$, $C_s(t)$, and $C_{I,out}(t)$ for the three-compartment model ($\dot{V}_{aw\,NO} \neq \dot{V}_{aw\,NO,U} > \dot{V}_{aw\,NO,L}$), with $\dot{V}_{aw\,NO}$ = 2,500 pl/s, $\bar{C}_A$ = 3.2 ppb, and $\dot{V}_{aw\,NO,L}$ = 1,000 pl/s, which implies $\dot{V}_{aw\,NO,U}$ = 16,000 pl/s (see APPENDIX A). Initially, the three-compartment model predicts a relatively steep phase II slope for $C_M(t)$ (corresponding to expired air from the upper airway section), which decreases significantly as air originating from the lower airway section appears at the mouth. Thus, during phase II, $C_M(t)$ is described by one- and two-line segments for the two- and three-compartment models, respectively. This results in higher levels of NO for $C_M(t)$, $C_s(t)$, and $C_{I,out}(t)$, particularly during phase II.

The impact of the instrument response is minimal [compare $C_{I,in}(t)$ with $C_{I,out}(t)$ in Fig. 2*B*]. However, substantial signal distortion results from NO transport through the sampling line [compare $C_M(t)$ and $C_s(t)$ with $C_{I,in}(t)$ in Fig. 2*B*]. Under these conditions, although the two-compartment model predicts steep leading phase II peaks for both $C_M(t)$ and $C_s(t)$, the expected response, $C_{I,out}(t)$, is flattened considerably and actually exhibits a trailing peak during phase III (see Fig. 2*B*). Often, this behavior was not observed in the experimental data. The three-compartment model elevates NO levels, during phase II for $C_M(t)$ and $C_s(t)$, and during both phase II and the beginning of phase III for $C_{I,out}(t)$ (see Fig. 2*C*). This effect is most pronounced for relatively small values of $\bar{C}_A$ and when $\dot{V}_{aw\,NO,U} \gg \dot{V}_{aw\,NO,L}$. Figure 2, *D* and *E*, shows the expected response, $C_{I,out}(t)$, for fixed $\dot{V}_{aw\,NO}$ = 2,500 pl/s and various values of $\dot{V}_{aw\,NO,U}$ and $\dot{V}_{aw\,NO,L}$, with $\bar{C}_A$ = 3.2 and 1.0 ppb, respectively. The additional degree of freedom provided by two airway sections enhances the three-compartment model's ability to fit experimental data. For example, with $\dot{V}_{aw\,NO}$ = 2,500 pl/s and C_A = 1.0 ppb, the three-compartment model predicts a peak concentration of NO in phase II for both

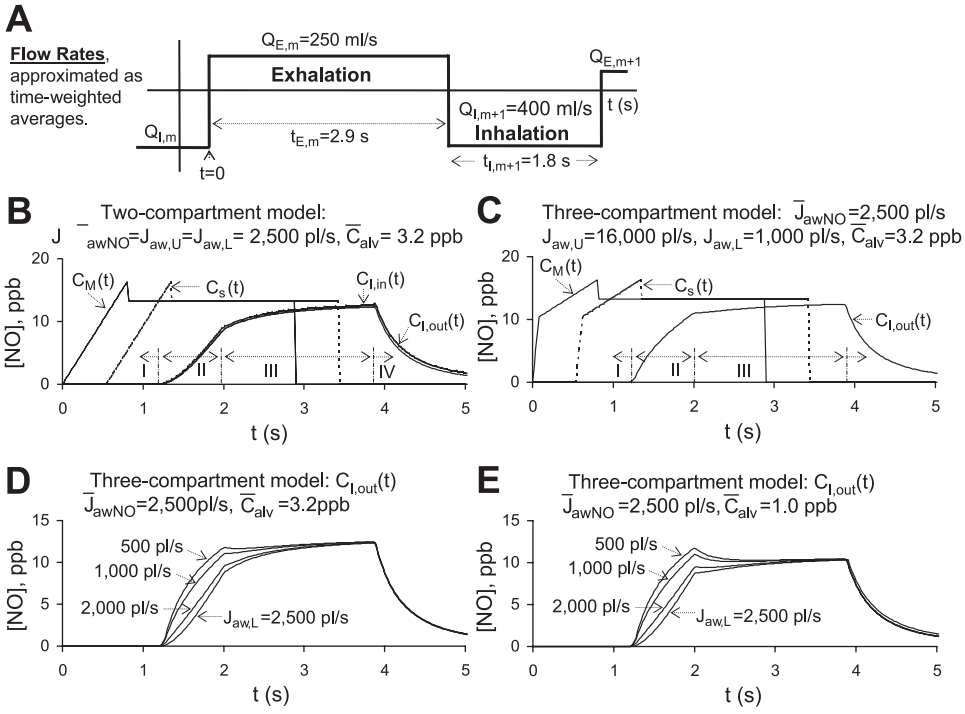

Fig. 2. Theoretical NO profiles for a single tidal breath, based on $\dot{V}_{awNO}$ = 2,500 pl/s, $\bar{C}_A$ = 1.0 or 3.2 parts/billion (ppb), and Vaw = 200 ml. *A*: time-weighted average flow rate profiles (Q_E = 250 ml/s, Q_I = 400 ml/s, t_E = 2.9 s, and t_I = 1.8 s, corresponding to $q_m = \dot{V}_{Im}/\dot{V}_{Em}$ = 1.6, f_{Bm} = 12.8 breaths/min, and $\dot{V}_{A_m}$ = 6.7 l/min). Observed exhalation profiles, $C_{I,out}(t)$, are described by 4 phases, designated by roman numerals: phase I (dead space), phase II (airway compartment), phase III (alveolar compartment), and phase IV (residual NO, observed during subsequent inhalation). NO concentration ([NO]) profiles are shown at the mouth, $C_M(t)$, sampling point, $C_s(t)$, inlet to NO analyzer, $C_{I,in}(t)$, and analyzer outlet, $C_{I,out}(t)$ (observed) with $\dot{V}_{awNO}$ = 2,500 pl/s and $\bar{C}_A$ = 3.2 ppb, for two-compartment model, $\dot{V}_{awNO,U} = \dot{V}_{awNO,L} = \dot{V}_{awNO}$ = 2,500 pl/s (*B*) and three-compartment model, $\dot{V}_{awNO,U}$ = 16,000 pl/s and $\dot{V}_{awNO,L}$ = 1,000 pl/s (*C*). $C_{I,out}(t)$ for three-compartment model is shown with $\dot{V}_{awNO}$ = 2,500 pl/s, $\dot{V}_{aw,L}$ = 500, 1,000, 2,000, and 2,500 pl/s for $\bar{C}_A$ = 3.2 ppb (*D*) and $\bar{C}_A$ = 1.0 ppb (*E*).

$J_{aw\,NO,L}$ = 500 and 1,000 pl/s (see Fig. 2*E*), which was often observed experimentally.

Comparison of predicted and experimental concentration profiles. Figure 3 shows observed and filtered data signals [$C_{obs}(t)$ and $\bar{C}_{obs}(t)$, respectively], as well as predicted concentration profiles, $C_s(t)$ and $\bar{C}_{I,out}(t)$, for typical individual breaths from *subjects 1* and *6*. Both examples demonstrate the smoothing achieved by filtering. The remaining fluctuations result from small variations in Q_E, gas-phase axial diffusion, or other phenomena, which are not included in the model.

Subject 1 (Fig. 3*A*) exhibits a single flat pulse for $C_s(t)$, and the efficacy of a significant baseline offset correction (nearly 2 ppb) is evident. Negative NO concentrations, resulting from a shift in instrument baseline during the course of an experiment, are compensated by least squares parameter estimation, which computes a constant "offset" for each breath. It would be very difficult to determine meaningful parameter estimates for *subject 1* without filtering and including the baseline correction, because observed NO concentration levels are close to the lower detection limits of the instrument. In contrast, for *subject 6* (Fig. 3*B*), the best fit to the data predicts a steep leading phase II peak for $C_s(t)$, which is flattened considerably by NO transport through the sampling line and the instrumentation response characteristics [compare $C_s(t)$ to $\bar{C}_{I,out}(t)$ and $\bar{C}_{obs}(t)$ and also see Fig. 2].

Figure 4 compares concentration profiles at the mouth, $C_M(t)$, determined theoretically based on the best fit of the data to the three-compartment model, and also by deconvolution (directly from the experimental data). Five tidal breaths are shown for *subjects 1* and *6* (Fig. 4, *A* and *B*, respectively), with $C_{obs}(t)$ included for reference. Both subjects exhibit a leading phase II peak for $C_M(t)$ and relatively flat phase III plateaus.

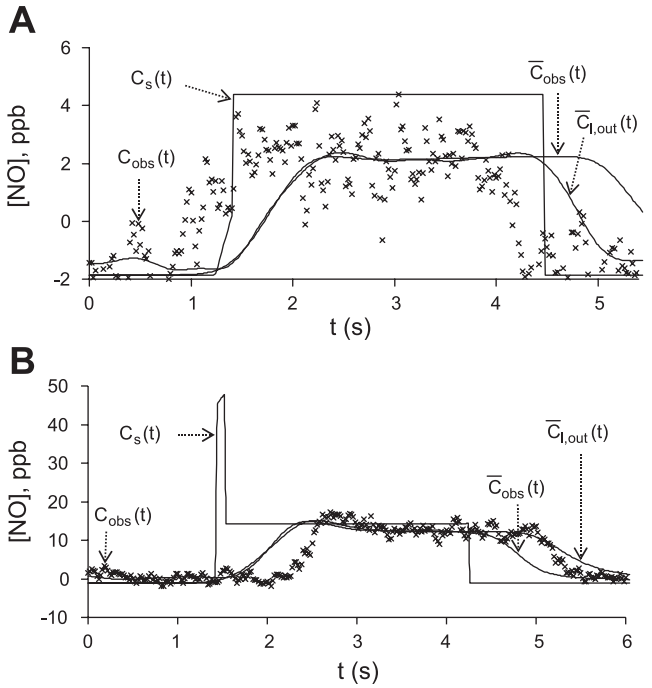

Fig. 3. Typical observed, $C_{obs}(t)$, filtered, $\bar{C}_{obs}(t)$, and predicted, $C_s(t)$ and $\bar{C}_{I,out}(t)$, NO exhalation profiles, determined by fitting $\bar{C}_{I,out}(t)$ to $C_{obs}(t)$ concentration profiles, for the individual breaths of *subject 1* (*A*) and *subject 6* (*B*).

Meaningful characterization of the leading phase II peak can only be achieved by assuming a heterogeneous NO production mechanism within the conductive airways, as proposed by the three-compartment model (i.e., $J_{aw\,NO,U} > J_{aw\,NO,L}$). Fluctuations, evident during phase III, would be even more prominent if $C_{obs}(t)$ were not prefiltered.

Parameter estimates from tidal breathing data. For all six subjects, a total of 282 tidal breaths were examined (Table 2). Of these, 68, 24, and 4 breaths were removed due to leakage of air from the mouthpiece, inadequate exhaled volume, or nasal contamination, respectively, as described in METHODS. Thus 186 breaths were analyzed for parametric characterization of NO exchange. Table 2 summarizes the specific data for each subject, including the f_B, $\dot{V}_A$ rate, and Q_I/Q_E. Table 3 summarizes the mean values and uncertainties for the tidal breathing parameters, $\bar{J}_{aw\,NO}$ and $\bar{C}_A$, as well as the mean breathing patterns for each subject. Clearly, $\bar{J}_{aw\,NO}$ is determined with reasonable precision (standard deviations range from 15–30% and standard errors from 2.3–7.5%). However, $\bar{C}_A$ is less well characterized (standard deviations range from 60–100% and standard errors from 10–24%).

Comparison of tidal breathing and single-breath parameters. Mean and standard deviations for the flow-independent parameters for the single-breath maneuvers are provided in Table 3. Ranges for standard deviations for $J'_{aw\,NO}$ and $C_{A_{NO}}$ are 14–28 and 24–132% and the range for standard errors are 10–20 and 17–93%, respectively. A plot of $\bar{J}_{aw\,NO}$ vs. $J'_{aw\,NO}$ is shown in Fig. 5*A* and $\bar{C}_A$ vs. $C_{A_{NO}}$ in Fig. 5*B* for the six subjects. There is a high degree of correlation (r^2 value > 0.95, P value < 0.001) for both pairs of parameters. The slope of $\bar{J}_{aw\,NO}$ vs. $J'_{aw\,NO}$ is 3.3 and is statistically >1.0 (line deviates to the *left* of the 45° line), and the slope for $\bar{C}_A$ vs. $C_{A_{NO}}$ is 0.45 and is statistically <1.0 (line deviates to the *right* of the 45° line).

Comparison of airway and alveolar parameters. A plot of $\bar{J}_{aw\,NO}$ vs. $\bar{C}_A$ from tidal breathing is shown in Fig. 5*C* for the six subjects and demonstrates a high degree of correlation (r^2 value = 0.99, P value < 0.001). However, single-breath parameters from the two-compartment model, $J'_{aw\,NO}$ and $C_{A_{NO}}$, are also highly correlated (r^2 value = 0.89, P value < 0.005, Fig. 5*D*).

DISCUSSION

This study has partitioned exhaled NO into airway and alveolar contributions by analyzing sequential tidal breaths and a three-compartment model of the lungs. The airway region is characterized by a volume-weighted flux of NO, $\bar{J}_{aw\,NO}$, which is analogous to the previously described $J'_{aw\,NO}$, determined from single-breath maneuvers (9, 17, 23, 27). The alveolar region is characterized by a $\bar{C}_A$, which is similar to $C_{A_{NO}}$, determined from single-breath maneuvers. Our results show that $\bar{J}_{aw\,NO}$ and $\bar{C}_A$ are well correlated with $J'_{aw\,NO}$ and $C_{A_{NO}}$, respectively (see Table 3 and Fig. 5). However, estimates of $\bar{J}_{aw\,NO}$ are significantly higher than those of $J'_{aw\,NO}$, and estimates of $\bar{C}_A$ are less than those of $C_{A_{NO}}$. These observations are likely due to altered gas-exchange dynamics in tidal breathing, which exploit simplifications in the lung model.

For single-breath maneuvers, such as those used in this study, which utilize a preexpiratory breath hold, accumulation of high-NO levels (>70 ppb) in the airway leads to a marked

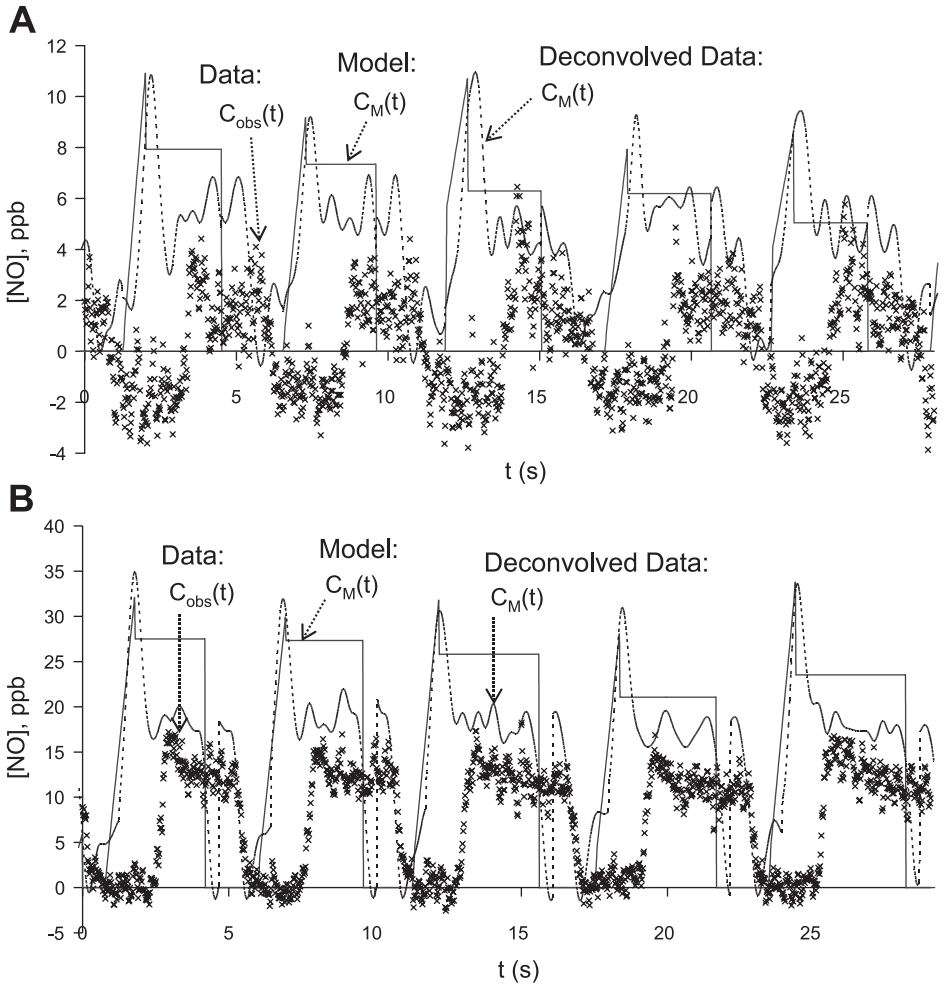

Fig. 4. Concentration profiles at the mouth, $C_M(t)$, determined based on best fit of data to pulmonary model and by deconvolution directly from experimental data. Five tidal breaths are shown, with observed data signal, $C_{obs}(t)$, included for reference, for *subject 1* (*A*) and *subject 6* (*B*).

peak observed at the beginning of exhalation (20, 27). During the breath hold, evidence of heterogeneous production of NO in the airway is mitigated due to axial or longitudinal diffusion, as well as the analysis technique, which considers only the total amount of NO exhaled in phases I and II (27). In contrast, a single tidal breath is completed within a shorter time interval, and much lower levels of NO are present within the airway compartment at the onset of exhalation, which results in a flat exhalation profile. In addition, heterogeneous rates of NO production in the airways become more prominent.

Consistent with this concept is our observation during tidal breathing of NO levels at the beginning of exhalation (phase I) that are higher than those predicted by the two-compartment model. Although low levels of nasal NO may have been present, breaths exhibiting NO concentrations exceeding 50 ppb were assumed to result from overt nasal contamination and were removed from our analysis. Thus, although a small level of nasal contamination cannot be ruled out, a more likely explanation is a higher rate of NO production in the upper airways, as described by other workers (5, 21, 24, 25). Thus the

Table 3. *Parameter estimates from single-breath and tidal breathing maneuvers*

	Single Breath with Preexpiratory Breath Hold			Tidal Breathing	
Subject No.	J'_{awNO}, pl/s	C_{ANO}, ppb	D_{awNO}, pl·s^{-1}·ppb^{-1}	$\bar{J}_{awNO}$, pl/s	$\bar{C}_A$, ppb
1	440(110)	1.3(1.2)	2.4(4.4)	1,500(300)	1.4(1.2)
2	330(92)	1.5(1.3)	2.0(3.7)	770(230)	1.5(1.0)
3	1,940(450)	21.6(6.9)	6.6(9.7)	7,600(1,600)	9.5(8.5)
4	340(79)	0.71(0.93)	7.1(4.4)	420(130)	0.3(0.3)
5	610(100)	1.8(1.3)	7.6(4.5)	1,000(200)	1.7(1.2)
6	1,510(220)	8.7(2.1)	2.1(1.9)	4,000(600)	4.6(2.8)
Mean ± SD	860 ± 690	5.9 ± 8.3	4.6 ± 2.7	2,500 ± 2,700	3.2 ± 3.4

Values are means with σ = composite uncertainty equivalent to standard deviation (see APPENDIX B) in parentheses. J'_{awNO}, maximum volumetric airway flux; C_{ANO}, steady-state alveolar concentration; D_{awNO}, airway diffusing capacity; $\bar{J}_{awNO}$, average volumetric conductive airway flux; $\bar{C}_A$, time-weighted average of alveolar concentration.

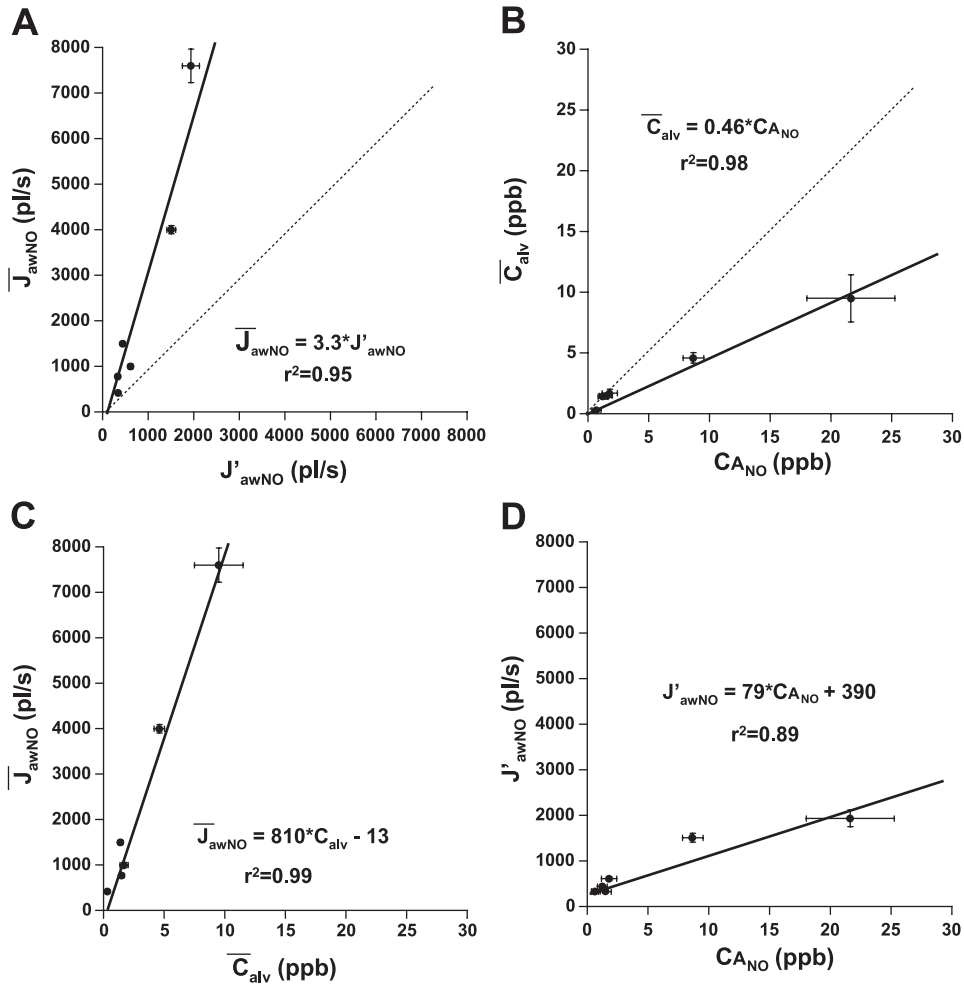

Fig. 5. Plots of mean parameter estimates determined for the 6 subjects. *A*: $\bar{J}_{awNO}$ vs. J'_{awNO}; *B*: $\bar{C}A$ vs. CA_{NO}; *C*: J'_{awNO} vs. $\bar{C}A$; and *D*: J_{awNO} vs. $\bar{C}A_{NO}$. Dotted lines in *A* and *B* represent the 45° line where independent and dependent variables have equivalent values. Solid lines represent best linear regression fit with corresponding r^2 value. For *A* and *B*, the intercept if fixed at zero (i.e., $\bar{J}_{awNO} = \beta \times J'_{awNO}$, where β is the slope), and for *C* and *D* the intercept is a variable. Error bars represent SE of the mean.

present study partitioned the airway compartment into an upper region (trachea and oropharynx) comprising 10% of the total Vaw, and a lower region comprising the remaining 90% of the Vaw. This representation leads to the three-compartment model (two airway compartments and one alveolar compartment).

We do not explicitly report estimates for $J_{aw\,NO,U}$ and $J_{aw\,NO,L}$; however, despite considerable intersubject variation and higher than expected estimates for $\bar{J}_{aw\,NO}$, their relative values (i.e., the ratios $J_{aw\,NO,U}/\bar{J}_{aw\,NO}$ and $J_{aw\,NO,L}/\bar{J}_{aw\,NO}$) are consistent with recently published experimental data for multiple-breath, constant-flow rate maneuvers (24) (data not shown). Further partitioning of the airway compartment is possible and may result in a more accurate prediction of the observed exhaled signal. However, this comes at the cost of additional unknown parameters. Although, based on previous experimental results, partitioning the airway into 10 and 90% fractions is arbitrary. Hence, alternate partitioning into different fractions should also be considered. In either case, the simple three-compartment model is capable of simulating higher NO levels at the beginning of exhalation.

Although the three-compartment model can successfully simulate the shape of experimental NO concentration profiles for tidal breathing, estimates for the volume-weighted NO flux within the airway compartment determined from tidal breathing data ($\bar{J}_{aw\,NO}$) are approximately threefold higher than estimates determined from single-breath maneuvers ($J'_{aw\,NO}$). In addition, estimates for the $\bar{C}A$ are smaller than those for CA_{NO} estimated from the single-breath maneuver. A possible explanation is the impact of axial diffusion of NO, which is neglected in the two- and three-compartment models. During a preexpiratory breath hold, NO excreted within the airway may be transported to the alveolar region by axial diffusion (i.e., "NO losses" to the alveolar compartment), resulting in reduced levels of NO in expired air (18, 29), reduced apparent airway wall flux of NO, and possibly an increase in the CA_{NO}. Because axial diffusion is neglected, the two-compartment model may underestimate $J'_{aw\,NO}$ by two- to fivefold (18, 29). However, tidal breathing allows much less time for axial diffusion to proceed, because inhalation is immediately proceeded by subsequent exhalation. Thus NO losses due to axial diffusion are likely to be significantly lower for tidal breathing than those for preexpiratory breath hold, resulting in a larger predicted airway compartment flux and a smaller alveolar concentration. Although gas flow mixing patterns and velocities differ between tidal breathing and a single-breath maneuver, radial NO transport between the airway wall and the air is tissue-phase limited (26). Thus there are no intrinsic reasons why the airway flux during tidal breathing would be larger than during a single breath, and future studies must consider axial diffusion in lung models as a potentially important mode of transport for NO.

Estimates of $\bar{J}_{aw\,NO}$ are correlated with those for $\bar{C}_A$ (see Fig. 5*C*), and estimates of $J'_{aw\,NO}$ are correlated with those for C_{ANO} (see Fig. 5*D*). Thus parameter estimates, corresponding to the conductive airways and alveolar regions, are dependent on each other for both single-breath and tidal-breathing maneuvers. This suggests that airway and alveolar NO are coupled either metabolically (i.e., subjects with higher airway NO production also produce more alveolar NO) or physically through mixing of gas from each compartment. For example, NO produced from the airways is transported to the alveolar region by convection and diffusion; thus a subject with high-airway NO production may artificially increase the alveolar NO concentration, leading to a positive correlation. These hypotheses may be addressed in future work through more advanced modeling (e.g., including axial diffusion) and experimental techniques.

It is clear that the signal-to-noise ratio in exhaled NO during tidal breathing is smaller than during a single-breath maneuver with a preexpiratory breath hold. However, data filtering, combined with analyzing multiple tidal breaths, can offset this disadvantage. Within a single subject, the standard deviation of the airway flux or the alveolar concentration is similar in tidal breathing and a single-breath maneuver (result of data filtering); however, the standard error of the estimate is substantially improved in tidal breathing due to the fact that many tidal breaths are sequentially analyzed (range of 19–52 breaths, mean of 31). In the case of the single-breath maneuver, only three breathing maneuvers are performed. It is also interesting to note that the time to collect 30 tidal breaths is similar to that to collect three single breaths (~5 min), yet no specific training or effort on the part of the subject is needed. The drawback of the tidal breathing analysis is the inability to estimate Daw_{NO}.

Our sampling system model accounts for important sources of time lags and distortion in tidal breathing, which are inherent to the experimental monitoring system (e.g., instrument response, laminar flow dispersion, transit times in plumbing, etc.). We have also corrected for misalignment of predicted and experimental concentration profiles. However, we have not attempted to optimize the analytic monitoring system. Our results suggest that monitoring system errors (e.g., mouthpiece lags and distortion in the sampling line) may significantly impact the shape of observed tidal breathing concentration profiles, and these errors propagate when multiple breaths are analyzed sequentially. Future investigation should lead to development of techniques for optimization of sampling system instrumentation and thus minimize the impact of systematic errors on experimental measurements.

The analysis of exhaled NO during tidal breathing provides an opportunity to characterize new subject populations who are incapable of performing single-breath maneuvers. Our results provide an initial assessment of tidal breathing to partition exhaled NO into airway and alveolar regions. Our analysis suggests that estimates of $\bar{J}_{aw\,NO}$ and $\bar{C}_A$ can provide region-specific information with improved accuracy (reduced standard error), yet less effort and training needed of the subject relative to the single-breath maneuver with a preexpiratory breath hold. Such information may be useful for detection of inflammatory diseases (e.g., asthma), which are characterized by additional NO production in the lower airways and alveolar region. Thus the assumption, $J_{aw\,NO,U} > J_{aw\,NO,L}$, may not hold for certain disease states (12, 21). Our simplified model does not include features such as axial diffusion or flow rate variability, which may be significant sources of error. Thus future work should focus on the development of more rigorous models, which will improve our characterization of NO gas exchange during tidal breathing. In addition, improved analytic instrumentation and implementation of more sophisticated filtering techniques may reduce the signal-to-noise ratio in the observed exhalation profile and thus further enhance parameter estimates. Despite these difficulties, the observation and analysis of multiple tidal breaths allows one to average parameter estimates, which offers a significant advantage relative to single-breath techniques.

APPENDIX A: PULMONARY AND MONITORING SYSTEM MODELS

Three-compartment model solution. With the use of time-weighted average flow rates for each breath, *m* ($Q_{I\,m}$ and $Q_{E\,m}$), *Eq. A1* can be solved analytically. The analytic solution was validated by applying a more rigorous solution [which accounts for time-dependent, flow-rate profiles in terms of airway residence time functions (26, 27)] to selected runs. Resetting $t = 0$ at the onset of each exhalation and applying the boundary condition, $C_{air}(t,V = 0) = \bar{C}_A$, *Eq. A1* is integrated to obtain the exhalation profile at the mouth, $C_M(t) = C_{air}(t,V = Vaw)$

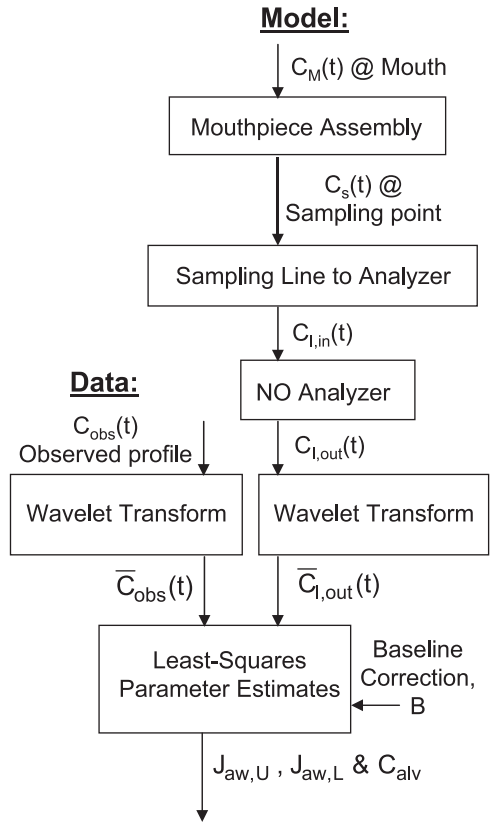

Fig. 6. Block flow diagram for quantitative analysis. Theoretical $C_M(t)$, at mouth, is corrected for time lags and residual NO in mouthpiece, to obtain $C_s(t)$, which is corrected for distortion, due to laminar flow and instrument response, by convolution to obtain $C_{I,out}(t)$. Wavelet transforms (prewhitening) are performed on $C_{I,out}(t)$ and the observed data signal, $C_{obs}(t)$, to obtain the filtered signals $\bar{C}_{I,out}(t)$ and $\bar{C}_{obs}(t)$, respectively, which are compared to determine least squares parameter estimates (intercept = baseline correction, *B*).

$$0 \le t < \tau_{Ea,U\,m}: C_M(t) = J_{aw\,NO,U}(1/Q_{E\,m} + 1/Q_{I\,m})t/\tau_{Ea\,m} \quad (A1)$$

$$\tau_{Ea,U\,m} \le t < \tau_{Ea\,m}: C_M(t) = (1/Q_{E\,m} + 1/Q_{I\,m}) \times [J_{aw\,NO,U}\tau_{Ea,U\,m} + J_{aw\,NO,L}(t - \tau_{Ea,U\,m})]/\tau_{Ea\,m} \quad (A2)$$

$$\tau_{Ea\,m} \le t < t_{E\,m}: C_M(t) = \bar{C}_A + \bar{J}_{aw\,NO}/Q_{E\,m} \quad (A3)$$

where $\tau_{Ea\,m} = Vaw/Q_{E\,m}$ and $\tau_{Ea,U\,m} = Vaw_U/Q_{E\,m}$ are the exhalation residence times of the entire airway and upper 10% of the airways, respectively; $Vaw = Vaw_U + Vaw_L$; and $Vaw\,\bar{J}_{aw\,NO} = Vaw_U\,J_{aw\,NO,U} + Vaw_L\,J_{aw\,NO,L}$ ($J_{aw\,NO,U}$, $J_{aw\,NO,L}$, and $\bar{C}_A$ are determined from experimental data). Because this implies that $Vaw_U = 0.1\,Vaw$ and $Vaw_L = 0.9\,Vaw$, if any two of the parameters, $\bar{J}_{aw\,NO}$, $J_{aw\,NO,U}$, and/or $J_{aw\,NO,L}$, are specified, the third parameter is fixed (i.e., $\bar{J}_{aw\,NO} = 0.1\,J_{aw\,NO,U} + 0.9\,J_{aw\,NO,L}$). If $J_{aw\,NO,U} = J_{aw\,NO,L} = \bar{J}_{aw\,NO}$, *Eqs. A1* and *A2* reduce to

$$0 \le t < \tau_{Ea\,m}: C_M(t) = \bar{J}_{aw\,NO}(1/Q_{E\,m} + 1/Q_{I\,m})t/\tau_{Ea\,m} \quad (A4)$$

The response of the mouthpiece assembly dead space is approximated as a plug flow; thus, at the sample point, $C_s(t) = C_M(t - \tau_{ds\,1m})$, for $0 < t < t_{E\,m}$. On subsequent inhalation ($t > t_{E\,m}$ and flow, $Q_{I\,m+1}$), NO-free air first traverses dead space volume, $V_{ds\,2}$. Thus, if $t_{E\,m} > \tau_{Ea\,m} + \tau_{E\,ds\,1m} + \tau_{E\,ds\,2m}$, *Eq. A3* implies $C_s(t) = \bar{C}_A + \bar{J}_{aw\,NO}/Q_{E\,m}$, for $t_{E\,m} \le t < t_{E\,m} + \tau_{I\,ds\,2,m+1}$ and C_s ($t > t_{E\,m} + \tau_{I\,ds\,2,m+1}$) = 0 (see Fig. 1*A*).

Expired air, entering the sample line ($V_s = 5.5$ ml, at $Q_s = 4.2$ ml/s, corresponding to space time, $\tau_s = V_s/Q_s \approx 1.3$ s), is maintained at laminar flow. This results in a delayed and distorted input to the analyzer, $C_{I,in}(t)$. Because the length-to-diameter ratio of the sample line is large, this effect is approximated in terms of a convolution integral (3)

$$t \le \tau_s/2: C_{I,in}(t) = 0 \quad (A5)$$

$$t > \tau_s/2: C_{I,in}(t) = (\tau_s^2/2)\int_0^{t-\tau_s/2} \frac{C_s(u)}{(t-u)^3}\,du \quad (A6)$$

The analyzer's response, $C_{I,out}(t)$, is modeled as a first-order system, characterized by the time constant, $\tau_A = 90$ ms (i.e., 200 ms required to reach 90% of full scale response), which is also a convolution integral (2)

$$C_{I,out}(t) = (1/\tau_A)\int_0^t C_{I,in}(u)e^{-(t-u)/\tau_A}du \quad (A7)$$

With $C_s(t)$ known and $C_{I,in}(t)$ determined from *Eqs. A5* and *A6*, numerical integration of *Eq. A7* yields $C_{I,out}(t)$ as the linear function of the model parameters: $C_{I,out}(t) = J_{aw\,NO,U}\,G_1(t) + J_{aw\,NO,L}\,G_2(t) + \bar{C}_A\,G_3(t)$, where $G_1(t)$, $G_2(t)$, and $G_3(t)$ are known (numerically determined) functions of time and breathing pattern. Thus $J_{aw\,NO,U}$, $J_{aw\,NO,L}$, and $\bar{C}_A$ are determined by fitting $C_{I,out}(t)$ to $C_{obs}(t)$. Alternatively, if $C_{I,out}(t)$ is specified, or its equivalent in terms of $C_{obs}(t)$, then $C_s(t)$ and $C_M(t)$ may be determined numerically, independent of the lung model, by deconvolution (analogous to numerical differentiation). Fluctuations in the observed experimental data make direct implementation of either convolution or deconvolution difficult. Fortunately, some of these fluctuations may be filtered from $C_{obs}(t)$ to facilitate these two techniques (see APPENDIX B).

APPENDIX B: DATA FILTERING, PARAMETER ESTIMATION, AND UNCERTAINTY ANALYSIS

Data filtering and parameter estimation. At low-NO levels, baseline fluctuations and other noise significantly impact the observed concentration signal. High-frequency noise was filtered from the observed signal (i.e., low-pass filtering) by comparing each set of tidal breathing data with its corresponding baseline and applying a Gaussian wavelet (Gabor) transform (13, 16). To avoid prejudice, we filter both $C_{obs}(t)$ and $C_{I,out}(t)$, thereby obtaining two transformed signals, $\bar{C}_{obs}(t)$ and $\bar{C}_{I,out}(t)$, respectively

$$\bar{C}_{obs}(t) = \int_0^{t_{E\,m}+t_{I_{m+1}}} C_{obs}(u)\,\frac{\psi_s(t,u)}{E_s(t)}\,du \quad (B1)$$

$$\bar{C}_{I,out}(t) = \int_0^{t_{E\,m}+t_{I_{m+1}}} C_{I,out}(u)\,\frac{\psi_s(t,u)}{E_s(t)}\,du + B \quad (B2)$$

where $\psi_s(t,u) = \dfrac{e^{-0.5[(u-t)/s]^2}}{s\sqrt{2\pi}}$, $E_s(t) = \int_0^{t_{E\,m}+t_{I\,m+1}} \psi_s(t,u)du$, s is a scaling facor (s = 0.1–0.3 s, for filtration frequencies of 1–3 Hz, respectively), and B is a correction for baseline drift (i.e., equivalent to a crude high-pass filter correction).

With $C_{I,out}(t)$ determined from *Eqs. A1*, *A2*, *A3*, *A5*, and *A7*, *Eq. B2* yields

$$\bar{C}_{I,out}(t) = J_{aw\,NO,U}\bar{G}_1(t) + J_{aw\,NO,L}\bar{G}_2(t) + \bar{C}_A\bar{G}_3(t) + B \quad (B3)$$

where $\bar{G}_1(t)$, $\bar{G}_2(t)$, and $\bar{G}_3(t)$ are known, numerically determined functions of time.

We determine $J_{aw\,NO,U}$, $J_{aw\,NO,L}$, and $\bar{C}_A$ by minimizing the least squared error between $\bar{C}_{obs}(t)$ and $\bar{C}_{I,out}(t)$ and translate the time scale of $\bar{C}_{I,out}(t)$ to achieve the best fit, imposing the constraints $J_{aw\,NO,U} \ge J_{aw\,NO,L} \ge 0$ and $\bar{C}_A \ge 0$. The overall procedure is illustrated in Fig. 6. Alternatively, numerical deconvolution of $C_{obs}(t)$ yields $C_s(t)$ and $C_M(t)$ directly from the experimental data.

Uncertainty analysis. We report estimates of $\bar{J}_{aw\,NO}$ and $\bar{C}_A$ for each subject as the average values determined from each sequence of M tidal breaths, and $J'_{aw\,NO}$ and C_{ANO} from single-breath maneuver in triplicate, weighting each breath equally. Composite uncertainties, σ_j ($j = \bar{J}_{aw\,NO}$, $\bar{C}_A$, $J'_{aw\,NO}$, and C_{ANO}), are then computed as

$$\sigma_j^2 = s_j^2 + \sum_{m=1}^{M}(\sigma_{jm}^2) \quad (B4)$$

where s_j^2 is the variance of the means from the sequence of M tidal breaths or three single breaths, and σ_{jm} are the uncertainties of individual tidal breaths or single breaths at 68.3% confidence, based on the t-statistic (14). Thus σ_j is analogous to the standard deviation, but includes allowances for both breath-to-breath variation and individual breath distributions.

REFERENCES

1. **Alving K, Weitzberg E, and Lundberg JM.** Increased amount of nitric oxide in exhaled air of asthmatics. *Eur Respir J* 6: 1368–1370, 1993.
2. **Arieli R and Liew HDV.** Corrections for the response time and delay of mass spectrometers. *J Appl Physiol* 51: 1417–1422, 1981.
3. **Aris R.** *Elementary Chemical Reactor Analysis*. Soneham, MA: Butterworth, 1989.
4. **Barnes PJ and Kharitonov SA.** Exhaled nitric oxide: a new lung function test. *Thorax* 51: 233–237, 1996.
5. **DuBois AB, Kelley PM, Douglas JS, and Mohsenin V.** Nitric oxide production and absorption in trachea, bronchi, bronchioles, and respiratory bronchioles of humans. *J Appl Physiol* 86: 159–167, 1999.
6. **Gaston B.** Expired nitric oxide in pediatric asthma: emissions testing for children? *J Pediatr* 131: 343–344, 1997.
7. **Girgis RE, Gugnani MK, Abrams J, and Mayes MD.** Partitioning of alveolar and conducting airway nitric oxide in scleroderma lung disease. *Am J Respir Crit Care Med* 165: 1587–1591, 2002.
8. **Hall GL, Reinmann B, Wildhaber JH, and Frey U.** Tidal exhaled nitric oxide in healthy, unsedated newborn infants with prenatal tobacco exposure. *J Appl Physiol* 92: 59–66, 2002.
9. **Hogman M, Drca N, Ehrstedt C, and Merilainen P.** Exhaled nitric oxide partitioned into alveolar, lower airways and nasal contributions. *Respir Med* 94: 985–991, 2000.
10. **Hogman M, Holmkvist T, Wegener T, Emtner M, Andersson M, Hedenstrom H, and Merilainen P.** Extended NO analysis applied to

patients with COPD, allergic asthma and allergic rhinitis. *Respir Med* 96: 24–30, 2002.
11. **Hogman M, Stromberg S, Schedin U, Frostell C, Hedenstierna G, and Gustaffson LE.** Nitric oxide from the human respiratory tract efficiently quantified by standardised single breath measurements. *Acta Physiol Scand* 159: 345–346, 1997.
12. **Hyde RW, Geigel EJ, Olszowka AJ, Krasney JA, Forster RE 2nd, Utell MJ, and Frampton MW.** Determination of production of nitric oxide by lower airways of humans–theory. *J Appl Physiol* 82: 1290–1296, 1997.
13. **Kaiser WM.** *A Friendly Guide to Wavelets*. Boston, MA: Birkhauser, 1994.
14. **Koch KR.** *Parameter Estimation and Hypothesis Testing in Linear Models*. New York: Springer-Verlag, 1999.
15. **Lehtimäki L, Kankaanranta H, Saarelainen S, Hahtola P, Järvenpää R, Koivula T, Turjanmaa V, and Moilanen E.** Extended exhaled NO measurement differentiates between alveolar and bronchial inflammation. *Am J Respir Crit Care Med* 163: 1557–1561, 2001.
16. **Otnes RK and Enochson L.** *Applied Time Series Analysis*. New York: Wiley, 1978.
17. **Pietropaoli AP, Perillo IB, Torres A, Perkins PT, Frasier LM, Utell MJ, Frampton MW, and Hyde RW.** Simultaneous measurement of nitric oxide production by conducting and alveolar airways of humans. *J Appl Physiol* 87: 1532–1542, 1999.
18. **Shin HW and George SC.** Impact of axial diffusion on nitric oxide exchange in the lungs. *J Appl Physiol* 93: 2070–2080, 2002.
19. **Shin HW, Rose-Gottron CM, Cooper DM, Newcombe RL, and George SC.** Airway diffusing capacity of nitric oxide and steroid therapy in asthma. *J Appl Physiol* 96: 65–75, 2004.
20. **Shin HW, Rose-Gottron CM, Perez F, Cooper DM, Wilson AF, and George SC.** Flow-independent nitric oxide exchange parameters in healthy adults. *J Appl Physiol* 91: 2173–2181, 2001.
21. **Silkoff PE, McClean PA, Caramori M, Slutsky AS, and Zamel N.** A significant proportion of exhaled nitric oxide arises in large airways in normal subjects. *Respir Physiol* 113: 33–38, 1998.
22. **Silkoff PE, McClean PA, Slutsky AS, Furlott HG, Hoffstein E, Wakita S, Chapman KR, Szalai JP, and Zamel N.** Marked flow-dependence of exhaled nitric oxide using a new technique to exclude nasal nitric oxide. *Am J Respir Crit Care Med* 155: 260–267, 1997.
23. **Silkoff PE, Sylvester JT, Zamel N, and Permutt S.** Airway nitric oxide diffusion in asthma. Role in pulmonary function and bronchial responsiveness. *Am J Respir Crit Care Med* 161: 1218–1228, 2000.
24. **Tornberg DC, Bjorne H, Lundberg JO, and Weitzberg E.** Multiple single breath measurements of nitric oxide in the intubated patient. *Am J Respir Crit Care Med* 168: 1210–1215, 2003.
25. **Tornberg DC, Marteus H, Schedin U, Alving K, Lundberg JO, and Weitzberg E.** Nasal and oral contribution to inhaled and exhaled nitric oxide: a study in tracheotomized patients. *Eur Respir J* 19: 859–864, 2002.
26. **Tsoukias NM and George SC.** A two-compartment model of pulmonary nitric oxide exchange dynamics. *J Appl Physiol* 85: 653–666, 1998.
27. **Tsoukias NM, Shin HW, Wilson AF, and George SC.** A single breath technique with variable flow rate to characterize nitric oxide exchange dynamics in the lungs. *J Appl Physiol* 91: 477–487, 2001.
28. **Tsoukias NM, Tannous Z, Wilson AF, and George SC.** Single-exhalation profiles of NO and CO_2 in humans: effect of dynamically changing flow rate. *J Appl Physiol* 85: 642–652, 1998.
29. **Van Muylem A, Noel C, and Paiva M.** Modeling of impact of gas molecular diffusion on nitric oxide expired profile. *J Appl Physiol* 94: 119–127, 2003.